Microchimica Acta (2022) 189: 30
https://doi.org/10.1007/s00604-021-05129-w

ORIGINAL PAPER

Photothermal-enhanced peroxidase-like activity of CDs/PBNPs for the detection of Fe^{3+} and cholesterol in serum samples

Yongxin Song[1] · Wenquan Liu[1] · Xin Mu[1] · Xiahua Zhong[1] · Anni Cui[1] · Yu Sun[1] · John R. Crockett[2] · Ying Bao[2] · Guiye Shan[1] · Yanwei Chen[1]

Received: 23 July 2021 / Accepted: 5 December 2021 / Published online: 16 December 2021
© The Author(s), under exclusive licence to Springer-Verlag GmbH Austria, part of Springer Nature 2021

Abstract

Carbon dots/Prussian blue nanoparticles (CDs/PBNPs) with fluorescence (FL) performance and peroxidase-like activity are synthesized by a simple two-step method. The FL of CDs/PBNPs can be effectively quenched by Fe^{3+}. Fe^{3+} can accelerate the peroxidase-like activity of CDs/PBNPs. More excitingly, the peroxidase-like activity of CDs/PBNPs could be further enhanced due to the influence of the photothermal effect. Based on the FL property and enhanced peroxidase-like activity, a cascade strategy is proposed for detection of Fe^{3+} and free cholesterol. CD/PBNPs act as FL probe for detection of Fe^{3+}. The enhanced peroxidase-like activity of CDs/PBNPs can also be used as colorimetric probe for the detection of free cholesterol. The detection ranges of Fe^{3+} and free cholesterol are 4–128 μM and 2–39 μM, and the corresponding limit of detections are 2.0 μM and 1.63 μM, respectively. The proposed strategy has been verified by the feasibility determination of Fe^{3+} and free cholesterol, suggesting its potential in the prediction of disease.

Keywords CDs/PBNPs · Peroxidase-like activity · Photothermal effect · Fluorescence probe · Cholesterol · Fe^{3+} determination

Introduction

The imbalance of Fe^{3+} and cholesterol in the body can cause many diseases such as Alzheimer's disease, anemia hemochromatosis, hypertension, and stroke [1–8]. Therefore, it is of great significance to detect the concentration of Fe^{3+} and cholesterol in serum. So far, although various analytical methods, including colorimetry [9, 10], fluorometry [11, 12], electrochemistry [13, 14], and atomic absorption spectrometry [15], have been reported for detection of Fe^{3+} and cholesterol, these methods require separate reagents and target only one of Fe^{3+} and free cholesterol. Thus, it is still a challenge to design a straightforward strategy for the detection of Fe^{3+} and free cholesterol.

✉ Guiye Shan
shangy229@nenu.edu.cn

[1] Centre for Advanced Optoelectronic Functional Materials Research, Key Laboratory for UV Light-Emitting Materials and Technology of the Ministry of Education, Northeast Normal University, Changchun 130024, China

[2] Department of Chemistry, Western Washington University, Bellingham, WA 98225, USA

PBNPs with face-centered cubic lattice have attracted great interest in phototherapy due to their strong absorption in the near-infrared spectrum [16–20]. However, as peroxidase mimic, PBNPs received little attention in colorimetric biosensing on account of their poor peroxidase-like activity [21–24]. The introduction of laser was proposed as a novel strategy to accelerate the catalytic activity of nanozymes [25, 26]. Due to Arrhenius formula, nanozymes with near-infrared light absorption could convert near-infrared light energy into internal energy under laser irradiation, which could improve their catalytic activity [25]. Another convenient strategy is to construct nanocomposites. The construction of nanocomposites could integrate the preponderance of each component and achieve the synergistic effect [27].

Carbon dots (CDs) are gaining wide attention because of their large specific area, excellent optical properties, and tunable surface chemistry [28–31]. The construction of nanocomposites based on CDs showed enhanced-catalytic abilities. For example, CDs served as capping and reducing agents to construct silver nanoparticles [32]. The synthesized carbon silver nano-assembly showed enhanced peroxidase-like activity and provided a colorimetric analysis for the sensitive detection of H_2O_2 and glucose. The loading

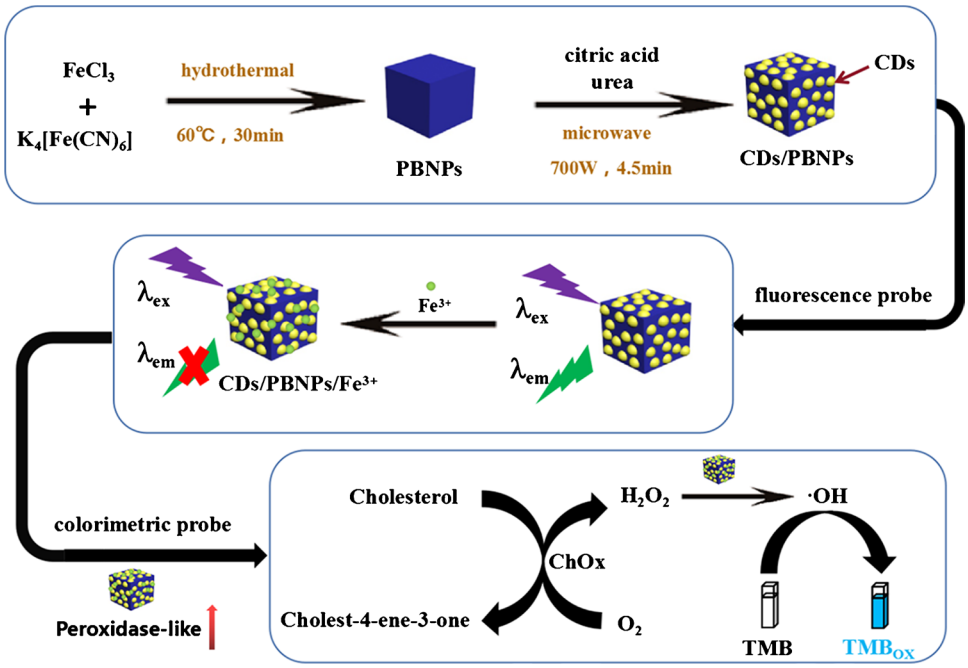

Scheme 1. Schematic illustration for the construction of CDs/PBNPs and the detection strategy of Fe^{3+} and free cholesterol

of carbon quantum dots increased the electrocatalytic surface area of octahedral cuprous oxide nanocomposites and improved the electrochemical stability and sensitivity of octahedral cuprous oxide nanocomposites, which enhanced their electrocatalytic activities [33]. In addition, due to the photo-induced electron transfer between Fe^{3+} ions and CDs, the FL of CDs can be effectively quenched by Fe^{3+} [34–40]. So, CDs could also act as FL probe for the detection of Fe^{3+}.

Herein, CDs/PBNPs were synthesized through a hydrothermal-assisted process followed by a microwave-assisted carbonation process. The synthesized CDs/PBNPs exhibited FL property and enhanced peroxidase-like activity. Interestingly, Fe^{3+} can also enhance the peroxidase-like activity of CDs/PBNPs, which was attributed to the cooperation between CDs/PBNPs and Fe^{3+}. Moreover, under laser irradiation, the peroxidase-like activity can be further improved by 10.9 times. Hence, a cascade strategy was designed for detection of Fe^{3+} and cholesterol (Scheme 1). Concretely, the synthetic CDs/PBNPs were used as FL probe for detection of Fe^{3+}. Then, the further enhanced peroxidase-like activity of CDs/PBNPs was served as colorimetric probe for determination of cholesterol in the presence of TMB and cholesterol oxidase. Furthermore, the reliability of this strategy in serum samples was also verified.

Experimental

Chemicals

$K_4[Fe(CN)_6]$ was obtained from Tian Jin Guangfu Technology Development Co., Ltd. (Tianjin, China). Iron(III) chloride hexahydrate ($FeCl_3{\cdot}H_2O$), urea (CH_4N_2O) and 30% hydrogen peroxide (H_2O_2) calcium chloride ($CaCl_2$), stannous chloride dihydrate ($SnCl_2{\cdot}2H_2O$), cobaltous nitrate hexahydrate ($Co(NO_3)_2{\cdot}6H_2O$), zinc nitrate hexahydrate ($Zn(NO_3)_2{\cdot}6H_2O$), sodium chloride (NaCl), potassium chloride (KCl), ammonium nitrate (NH_4NO_3), dibasic sodium phosphate, (Na_2HPO_4), potassium dihydrogen phosphate (KH_2PO_4), nitric acid (HNO_3), 2-aminoethanol, histidine, and arginine were provided from Sinopharm Chemical Reagent Co., Ltd. (Beijing, China). The citric acid (CA), ethanol (CH_3CH_2OH), acetic acid, glycerin, and glucose purchased from Beijing Chemical Works Co. Ltd. (Beijing, China). 3,3′,5,5′-tetramethylbenzidine (TMB), dopamine, and ascorbic acid were purchased from Sigma-Aldrich. Cholesterol oxidase (ChOx), cholesterol, Tri(hydroxymethyl) amino methane hydrochloride (Tris–HCl), and 5,5-dimethyl-1-pirroline-*N*-oxide (DMPO) came from Shanghai Yuanye Bio-Technology Co., Ltd. (Shanghai, China).

Instrumentations

The morphology of CDs/PBNPs was tested by Transmission electron microscopy (TEM) Tecnai F20 (FEI, USA) and high-angle annular dark-field scanning transmission electron microscopy (HAADF-STEM) JEM-2100F (JEOL, Japan). The UV–vis and Fourier transform infrared (FT-IR) spectrum of CDs/PBNPs were conducted on UV2600 spectrophotometer (Shimadzu, Japan) and Nicolet iS10 FT-IR spectrometer (Thermo fisher, USA), respectively. The hydrodynamic size and zeta potential were collected

on a Zetasizer Nano ZS90 (Malvern, England). The X-ray diffraction (XRD) pattern of CDs/PBNPs was carried out by a Rigaku D/max-2500 XRD (Rigaku, Japan). The FL spectra of CDs/PBNPs were gotten from a PTI-QuantaMaster 400 (PTI, USA). Electron spin resonance (ESR) spectra were measured by Bruker EMXnano Electron Paramagnetic Resonance spectrometer (Billerica, USA).

Synthesis of PBNPs

$FeCl_3$ (3.2 mg) and CA (107 mg) were added to 20 mL of deionized water. Then, 20 mL of deionized water deionized water containing $K_4[Fe(CN)_6]$ (8.4 mg) and CA (107 mg) was added dropwise into the above solution under vigorous stirring at 60 °C. A bright blue color rapidly appeared during the blending process. The reaction was maintained for 5 min and cooled down to 20 ℃ for another 30 min. The PBNPs precipitation was obtained by centrifugation (12,000 rpm, 30 min) three times with ethanol after the reaction. Finally, the obtained PBNPs precipitation was dried overnight under vacuum at room temperature.

Synthesis of CDs/PBNPs

In brief, CA (270 mg), urea (90 mg) and PBNPs (10 mg) were dissolved in deionized water (10 mL) and then heated in the microwave (700 W) for 5 min. The products were dissolved in 10 mL of deionized water, followed by centrifuging (12,000 rpm, 30 min) five times with deionized water and drying under vacuum at 40 °C.

Calculation of quantum yield

The quantum yields of CDs/PBNPs were determined by comparing the integrated FL intensities ($\lambda_{ex} = 360$ nm) and the absorbance of CDs/PBNPs ($\lambda = 360$ nm) with that of quinine sulfate. In brief, quinine sulfate (0.1 M H_2SO_4, quantum yield is 54%) solution, considered as a standard solution, diluted with ultrapure water to five different concentrations for the absorbance tests. The absorption values of these solutions were kept below 0.1 at the excitation wavelength (360 nm) to minimize the re-absorption effects. The quantum yields were calculated according to the following formula:

$$QY_S = QY_R \times \left[I_s \times A_R \times \eta s^2\right] / \left[I_R \times As \times \eta_R^2\right] \quad (1)$$

where QY_S and QY_R are the quantum yields of CDs/PBNPs and the reference compound (quinine sulfate). I is the integrated FL emission intensity, A is the absorbance value at the excitation wavelength, and η is the refractive index of the solvent ($\eta_S/\eta_R = 1$). The subscript "S" and "R" are the sample and the reference compound.

Detection of Fe^{3+}

Firstly, the selectivity of CDs/PBNPs for Fe^{3+} detection was determined by testing the quenching performance of CDs/PBNPs in the presence of different metal ions. Typically, 0.5 mL of metal ion (6 mM) solution was added into 2.5 mL of phosphate buffer saline (PBS, 0.1 M, pH 7.4) containing CDs/PBNPs (12 μg/mL). The mixed solution was incubated for 15 min, and then the emission FL spectra were detected by the FL detector at the excitation wavelength of 420 nm. The FL intensity of CDs/PBNPs solution in the presence of Fe^{3+} co-existing with other different metal ions was also measured. 0.5 mL of Fe^{3+} (6 mM) containing other metal ion (6 mM) was added into 2.5 mL of CDs/PBNPs solution (12 μg/mL). The sensitivity and pH-dependent FL property of CDs/PBNPs for detection of Fe^{3+} was evaluated by adding different concentrations of Fe^{3+} (diluted with PBS) and different PBS (pH 1–11) in the same way. Moreover, the kinetic behavior of the quenching pattern was further evaluated by recording the FL intensity of CDs/PBNPs (10 μg/mL) with the addition of Fe^{3+} (1 mM) in real time. The FL emission spectrum was obtained with the excitation wavelength of 420 nm.

Peroxidase-like activity

TMB was used to investigate the peroxidase-like performance of CDs/PBNPs. CDs/PBNPs can catalyze the colorless TMB to the blue oxidized TMB which has a specific absorption at $\lambda = 652$ nm. Specifically, experiments were carried out by mixing 2800 μL of acetate buffer (0.1 M, pH 7.4) containing CDs/PBNPs (3 μg/mL) and different concentrations of 100 μL of TMB and 100 μL of H_2O_2 (diluted with acetate buffer solution). Kinetic measurements were performed by monitoring the absorption of oxidized TMB at $\lambda_{max} = 652$ nm in real-time.

The effects of pH and temperature on the peroxidase-like activity of PBNPs and CDs/PBNPs were also evaluated using the above procedures. Briefly, 2800 μL of PBS (0.1 M, pH 2–11) containing CDs/PBNPs (3 μg/mL), 100 μL of TMB (1 mM), and 100 μL of H_2O_2 (1 mM) were incubated at 37 °C for 10 min. The peroxidase-like activity was measured by recording the absorption at $\lambda_{max} = 652$ nm. Likewise, the effects of temperature on peroxidase-like activity were evaluated at 10–50 °C (pH 6). The stability of CDs/PBNPs was evaluated by measuring the changes of particle size and FL in two months.

Detection of ROS

DMPO was chose to detect the hydroxyl radicals in PBNPs and CDs/PBNPs systems. Two hundred μL system containing PBNPs (10 μg/mL), H_2O_2 (1 mM), and DMPO (5 mM) were added to a glass capillary and then sealed for 1 min. The ESR spectra were obtained by the ESR spectrometer.

Cooperation interaction of CDs/PBNPs and Fe^{3+}

Three thousand μL of PBS (0.1 M, pH 7.4) containing different concentrations of Fe^{3+} (0–40 μM), CDs/PBNPs (10 μg/mL), TMB (1 mM), and H_2O_2 (1 mM) was incubated for 10 min, and the UV–vis spectra were recorded. Then the UV–vis spectra of the mixture were recorded to evaluate the peroxidase-like activity of CDs/PBNPs. The cooperation interaction of CDs/PBNPs with other metal ions (Na^+, K^+, Ca^{2+}, Co^{2+}, Mn^{2+}, Zn^{2+}, Cu^{2+}, Fe^{2+}, Fe^{3+}) was evaluated in the same way.

Photothermal-enhanced peroxidase-like activity

One mL of solution containing CDs/PBNPs (10 μg/mL), H_2O_2 (1 mM), and TMB (1 mM) was irradiated by 808 nm laser (0.75 W/cm^2) for 120 s. The effect of laser on peroxidase-like activity was performed by monitoring the absorption of oxidized TMB at $\lambda_{max} = 652$ nm in real time. The effects of different power laser (0.5, 0.75, 1.25 W/cm^2) on peroxidase-like activity were measured in the same way. The changes of temperature during the laser irradiation were recorded using an infrared camera.

Detection of cholesterol

Cholesterol (0.0387 g) was dissolved in 10 mL of solution containing 10% ethanol, 10 % Triton X-100, and 80 % KH_2PO_4-K_2HPO_4 buffer (10 mM, pH 7.4) and diluted to different concentration solutions with the above mixed solution (10 % ethanol, 10 % Triton X-100, and 80 % KH_2PO_4-K_2HPO_4 buffer. Then, 50 μL of ChOx (10–20 U/mg) and 400 μL of the cholesterol solution were incubated at 37 ℃ for 30 min. After that, 50 μL of CDs/PBNPs (0.6 mg/mL), 100 μL of TMB (30 mM), and 2500 μL of NaAc-HAc buffer (100 mM, pH 7.4) were added and incubated for an additional 20 min. The change of absorption value was determined by UV 2600 spectrometer.

Detection of Fe^{3+} and free cholesterol in serums

The feasibility of this method was evaluated by detecting the levels of Fe^{3+} and free cholesterol in serums. The serums were provided by three healthy volunteers and stored at 4 ℃ before using.

For the determination of Fe^{3+}, all samples were first treated with HNO_3 to release Fe^{3+} from the proteins. One hundred μL of concentrated HNO_3 was added to 100 μL of the serum sample incubated for 2 h. After nitrification, the serum sample was centrifuged (5000 rpm, 10 min), and the supernatant was adjusted to neutral pH with NaOH solution (0.1 M). Then 20 μL of CDs/PBNPs (33 μg/mL) was added for 15 min of incubation at 37 ℃. The concentration of Fe^{3+} in the serum sample was calculated by measuring the FL emission spectra at 510 nm. For the free cholesterol determination, 100 μL of above serum, 100μL of the ChOx (10–20 U/mg), and 1800 μL of phosphate buffer containing 2.5 mM TMB (100 mM, pH 7.4) were incubated for half an hour at 37 ℃. The level of cholesterol in the serum sample was calculated by recording the absorbance value at 652 nm.

Results and discussion

Choice of materials

Prussian blue, a dye approved by FDA for the treatment of heavy metal poisoning, has attracted extensive attention due to its simple synthesis process, high surface tunability, and excellent biocompatibility. However, the poor peroxidase-like activity and dispersibility still restricts its application in colorimetric sensing. CDs possess excellent solubility in water, good biocompatibility, and outstanding optical property compared with conventional quantum dots (Cd and Se quantum dots). CD-based nanoparticles have showed enhanced peroxidase activity, such as AgNPs and Cu_2O [32. 33]. The construction of the environment friendly of PBNPs and CDs is expected to not only enhance the peroxidase activity of PBNPs, but also make PBNPs multi-functionalization.

Characterization of CDs/PBNPs

CDs/PBNPs were prepared by the two-step method. The TEM image of CDs shows a narrow size range from 4.6 to 7.0 nm (Fig. S1). The high-resolution TEM of CDs reveals the crystalline structure with the lattice parameter of 0.21 nm, which correspond to the C (100) facet of graphite (Fig. S1 inset). The TEM and HAADF-STEM images show the structural morphology of PBNPs and CDs/PBNPs. As shown in the TEM images, PBNPs are cubes with an average size of 46 nm (Fig. 1A and C). CDs/PBNPs evolve from cubes into irregular shapes of a larger average size (78 nm) (Fig. 1D and F). Moreover, the change of morphology is further supported by the HAADF-STEM image (Fig. 1B and E). According to the HAADF-STEM image of PBNPs, PBNP exhibits a cubic shape with uniform size (Fig. 1B). The bright spots areas and fuzzy edges of the CDs/PBNPs

are caused by the deposition of CDs on the surface of PBNPs (Fig. 1E).

The synthesized CDs/PBNP was further characterized by the XRD, FTIR spectroscopy, DLS, zeta potentials, UV–vis spectroscopy, and FL spectroscopy. As shown in Fig. 2A, the diffraction peaks of CDs/PBNPs at 17.4°, 24.5°, 35.2°, 39.5°, 43.6°, 50.6°, 54.2°, 57.2°, 66.1°, and 69.1° are well matched with the (200), (220), (400), (420), (422), (440), (600), (620), (640), and (642) planes of Prussian blue lattice (JCPDS No. 52–1907), indicating that CDs/PBNPs maintain the same cubic face-centered structure as PBNPs. The peak centered at around 27° in the XRD patterns of CDs/PBNPs is the intrinsic graphitic structure, which indicates the existence of CDs [16]. No additional impurities diffraction peaks were found, implying the high purity of the obtained product. As shown in the FTIR spectrum (Fig. 2B), CDs/PBNPs present four obvious bands. The band at 2070 cm^{-1} indicates the vibration signal of Fe^{3+}-N≡C-Fe^{2+}. The bands at 1712 and 1640 cm^{-1} are assigned to C = O stretching vibrations. The N–H bending vibrations are obtained at 1460 cm^{-1}. The broad bands around 3460 cm^{-1} are attributed to the stretching vibrations of N–H and O–H. Those absorption bands demonstrate the presence of lots of carboxyl, hydroxyl, and amino groups on the surface of CDs/PBNPs, which can stabilize the CDs/PBNPs in aqueous environment. Dynamic light scattering (DLS) was used to examine the change of particle size during the formation of CDs/PBNPs (Fig. 2C). The average hydrodynamic diameter of CDs, PBNPs, and CDs/PBNPs are about 7.5 nm, 58.8 nm, and 78.8 nm, respectively, which are consistent with the change observed in TEM and HAADF-STEM. Additionally, CDs/PBNPs maintain the stability of particle size after two months of storage at 4 ℃, which indicates that CDs/PBNPs is stable for the further application (Fig. S2). The change of zeta potential was studied during the assembly process (Fig. 2D). The zeta potential of CDs/PBNPs is − 21.0 mV, which is due to the attachment of positively charged CDs (+ 36.8 mV) onto the surface of negatively charged PBNPs (− 34.8 mV). CDs/PBNPs exhibits a typical UV–vis absorption band from 500 to 900 nm with a strong peak at around 700 nm (Fig. 2E), which is due to the intermetallic charge transfer between Fe^{2+} and Fe^{3+} in CDs/PBNPs. The peak at 420 nm is attributed to the n- π* transition of C = O groups in CDs. CDs and CDs/PBNPs emit visible yellow and green FL when excited with UV (365 nm) light, respectively (Fig. 2F inset). The emission of CDs/PBNPs is excitation-dependent in the excitation wavelength from 340 to 480 nm (Fig. S3). The maximum emission wavelength of CDs/PBNPs is at 510 nm upon the excitation wavelength at 420 nm, which are about 10 nm blue-shifted in relative to that of CDs (Fig. 2F). Moreover, the FL quantum yield of CDs/PBNPs was measured to be 12.7 % which was lower than that of CDs (37.9%). In

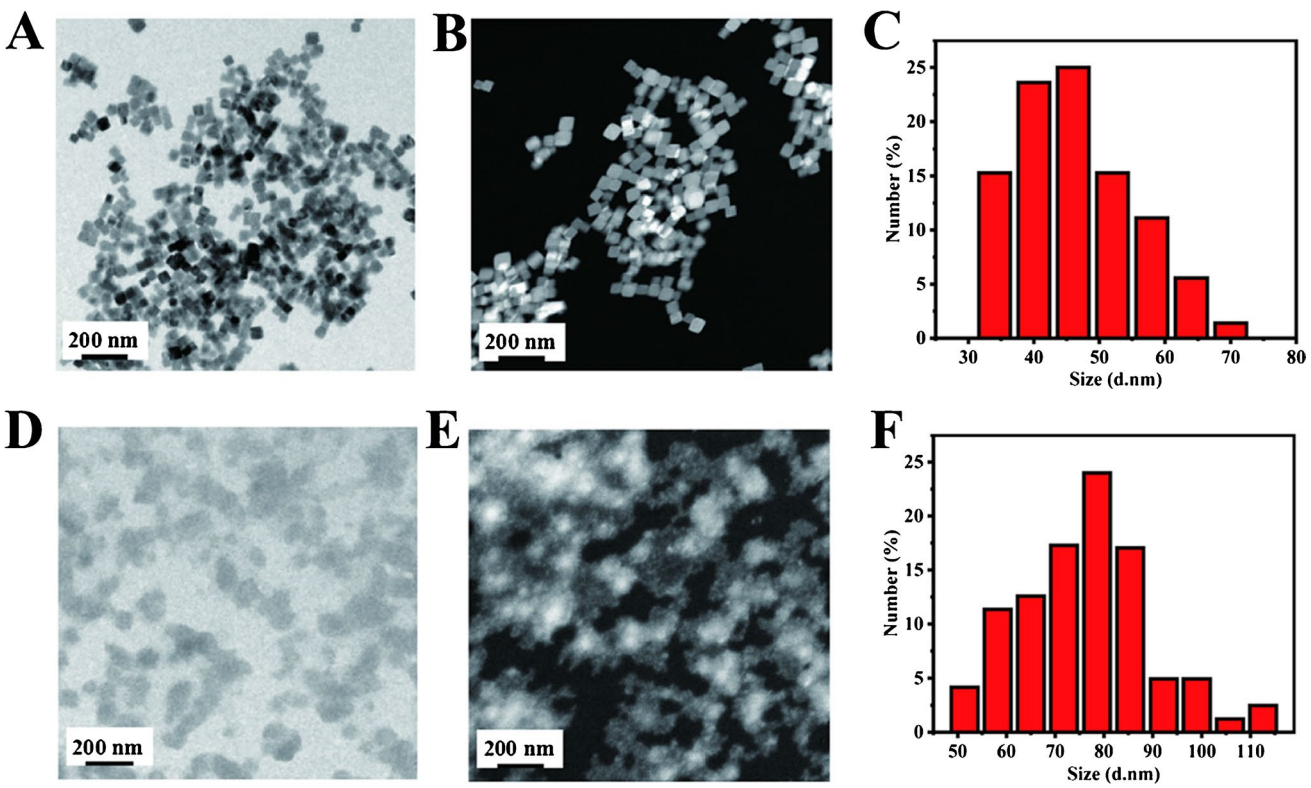

Fig. 1 (**A**) TEM image of PBNPs. (**B**) HAADF-STEM image of PBNPs. (**C**) Size distribution histogram of PBNPs obtained from (**A**). (**D**) TEM image of CDs/PBNPs. (**E**) HAADF-STEM image of CDs/PBNPs. (**F**) Size distribution histogram of CDs/PBNPs obtained from (**D**)

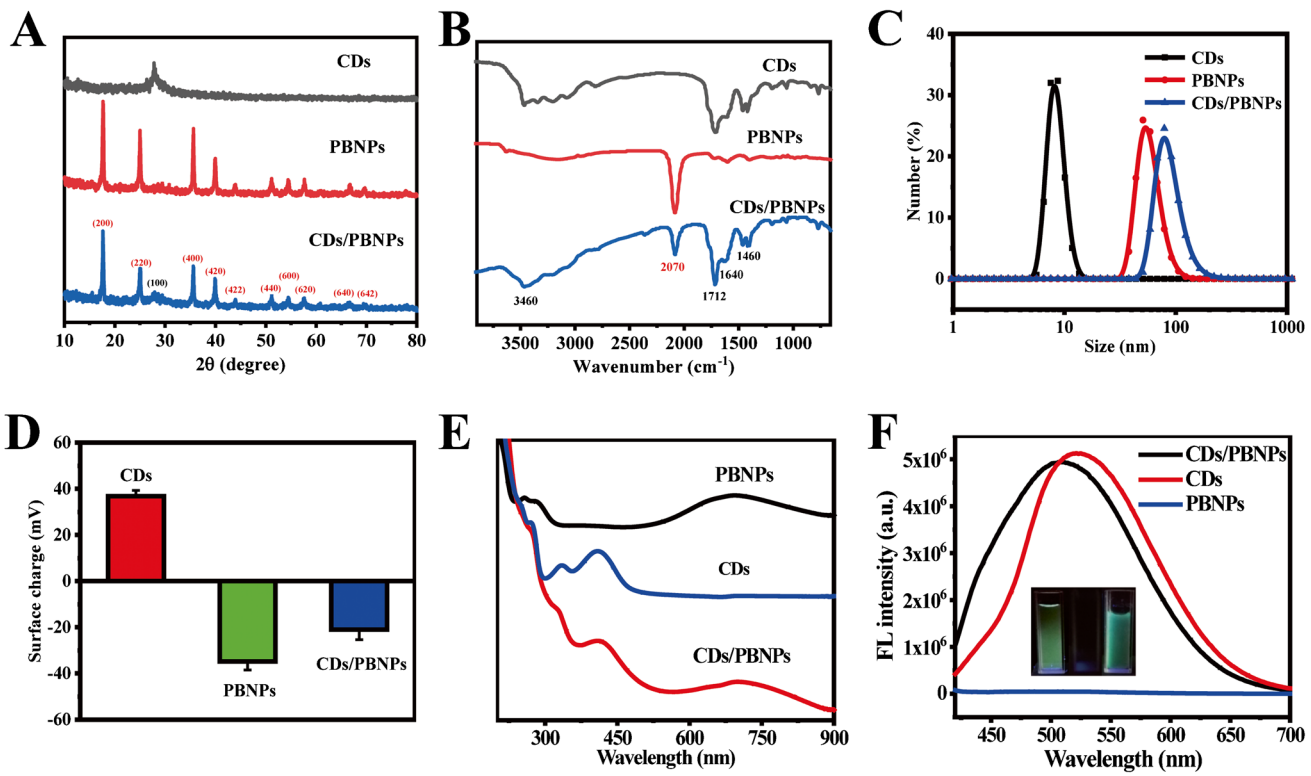

Fig. 2 XRD patterns (**A**), FTIR spectra (**B**), dynamic light scattering data (**C**), zeta potentials (**D**) of CDs, PBNPs, and CDs/PBNPs. UV–vis spectra of CDs (200 μg/mL), PBNPs (200 μg/mL), and CDs/PBNPs (200 μg/mL) (**E**). FL spectra of CDs (40 μg/mL), PBNPs (40 μg/mL), and CDs/PBNPs (40 μg/mL) (**F**). The FL spectrum was acquired at the excitation wavelength of 420 nm

addition, CDs/PBNPs still maintain the stability of FL after two months of storage at 4 ℃ (Fig. S4).

Peroxidase-like activity of CDs/PBNPs

C Steady-state kinetic assay of PBNPs (3 μg/mL) and CDs/PBNPs (3 μg/mL) for TMB in the presence of 1 mM H_2O_2. **D** Steady-state kinetic assay of PBNPs (3 μg/mL) and CDs/PBNPs (3 μg/mL) for H_2O_2 in the presence of 1 mM TMB. **E** Lineweaver–Burk plots of PBNPs (3 μg/mL) and CDs/PBNPs (3 μg/mL) for TMB in the presence of 1 mM H_2O_2. **F** Lineweaver–Burk plots of PBNPs (3 μg/mL) and CDs/PBNPs (3 μg/mL) for H_2O_2 in the presence of 1 mM TMB. Error bar represents the standard deviation for three determinations.

The intrinsic heme-like structure endowed PBNPs with enzyme-mimetic activity [22]. In order to compare the peroxidase-like activities of PBNPs and CDs/PBNPs, TMB was selected as the substrate. In the presence of H_2O_2, PBNPs could catalyze the colorless TMB to form the blue TMBox, which has strong absorption at λ = 652 nm. The peroxidase-like activities of CDs, PBNPs, and CDs/PBNPs are compared by monitoring the absorption of TMBox (Fig. 3A). CDs show no change in the present of TMB and H_2O_2, suggesting that CDs has no peroxidase-like activity. However, CDs/PBNPs exhibit higher peroxidase-like activity than that of PBNPs, which was consistent with the change of TMBox absorbance at λ = 652 nm (Fig. 3B).

The peroxidase-like kinetic processes of the PBNPs and CDs/PBNPs was further studied. The peroxidase-like dynamics were obtained from the Michaelis–Menten curve (Fig. 3C and 3D). The Michaelis–Menten constant (K_m) and maximum initial velocity (V_{max}) were obtained from the Lineweaver–Burk plot [22] (Fig. 3E and 3F). The K_m, the Michaelis constant, generally indicates the affinity between enzymes and substrates. The lower value of the K_m, the higher the affinity with the substrate. The K_m value of CDs/PBNPs towards TMB was smaller than PBNPs (Table 1), indicating that the affinity between CDs/PBNPs and TMB is stronger in comparison to that between PBNPs and TMB. In addition, CDs/PBNPs had higher V_{max} for H_2O_2 than PBNPs, which indicated that CDs/PBNPs required a higher H_2O_2 concentration to achieve the maximum activity.

The peroxidase-like activity of CDs/PBNPs is considered to be affected by pH and temperature [41]. The peroxidase-like activities of PBNPs and CDs/PBNPs are investigated in the range of pH from 2.0 to 11.0 (Fig. S5). CDs/PBNPs exhibit higher peroxidase-like activity than PBNPs. Under

alkaline pH from 8.0 to 11.0, PBNPs and CDs/PBNPs quickly lose their activities. It is due to the decomposition of the PBNPs by OH^- [41], which is confirmed by the decrease of absorbance at 712 nm with increasing pH (Fig. S6). The effect of reaction temperature was then investigated. Both of PBNPs and CDs/PBNPs were exposed to 10–50 ℃ (Fig. S7). The result showed that temperature could significantly affect the activity of PBNPs and CDs/PBNPs, and the optimum temperature for the catalytic reaction is 40 ℃.

In order to explore the mechanism of enhanced peroxidase-like activity of CDs/PBNPs, ESR spectrum was chosen to identify the generated active free radicals. In fact, Fe^{2+} and Fe^{3+} ions in the PBNPs can catalyze the reaction of H_2O_2 to produce hydroxyl radicals and exhibit peroxidase-like activity though the Fenton reaction [22].

$$Fe^{2+} + H_2O_2 \rightarrow Fe^{3+} + OH^- + \cdot OH \quad (2)$$

$$Fe^{3+} + H_2O_2 \rightarrow Fe^{2+} + H^+ + \cdot O_2H \quad (3)$$

As shown in Fig. S8, the PBNPs/DMPO/H_2O_2 and CDs/PBNPs/DMPO/H_2O_2 systems showed four obvious peaks, which were the typical peaks of hydroxyl radicals. However, the hydroxyl radical intensity of CDs/PBNPs was stronger than that of PBNPs, suggesting that CDs/PBNPs could produce more hydroxyl radical in the process of H_2O_2. Based on this result, the possible mechanism of the enhanced peroxidase-like activity of CDs/PBNPs could be attributed to the accelerated generation of hydroxyl radicals.

Table 1 Comparison of kinetic parameters of PBNPs and CDs/PBNPs

	Catalysts	PBNPs	CDs/PBNPs
K_m (mM)	TMB	0.598	0.311
	H_2O_2	1.767	3.457
V_{max} ($\mu M \cdot s^{-1}$)	TMB	0.0269	0.0588
	H_2O_2	0.0178	0.0612

Detection of Fe^{3+}

In order to investigate the selective sensing ability of CDs/PBNPs toward Fe^{3+}, ten different metal ions were used to study the FL quenching of CDs/PBNPs at 420 nm excitation wavelength (Fig. 4A). Compared with other metal ions, Fe^{3+} significantly quenched the FL of CDs/PBNPs, indicating that the selectivity of CDs/PBNPs toward Fe^{3+} over the other metal ions. In addition, the FL quenching effect is not affected by the coexistence of other metal ions (Fig. S9), indicating the strong affinity between CDs/PBNPs and Fe^{3+}. The FL intensity of CDs/PBNPs in PBS and Tris–HCl (100 mM, pH 7.4) was similar to that in water (Fig. 4B). CDs/PBNPs showed no significant effect on the

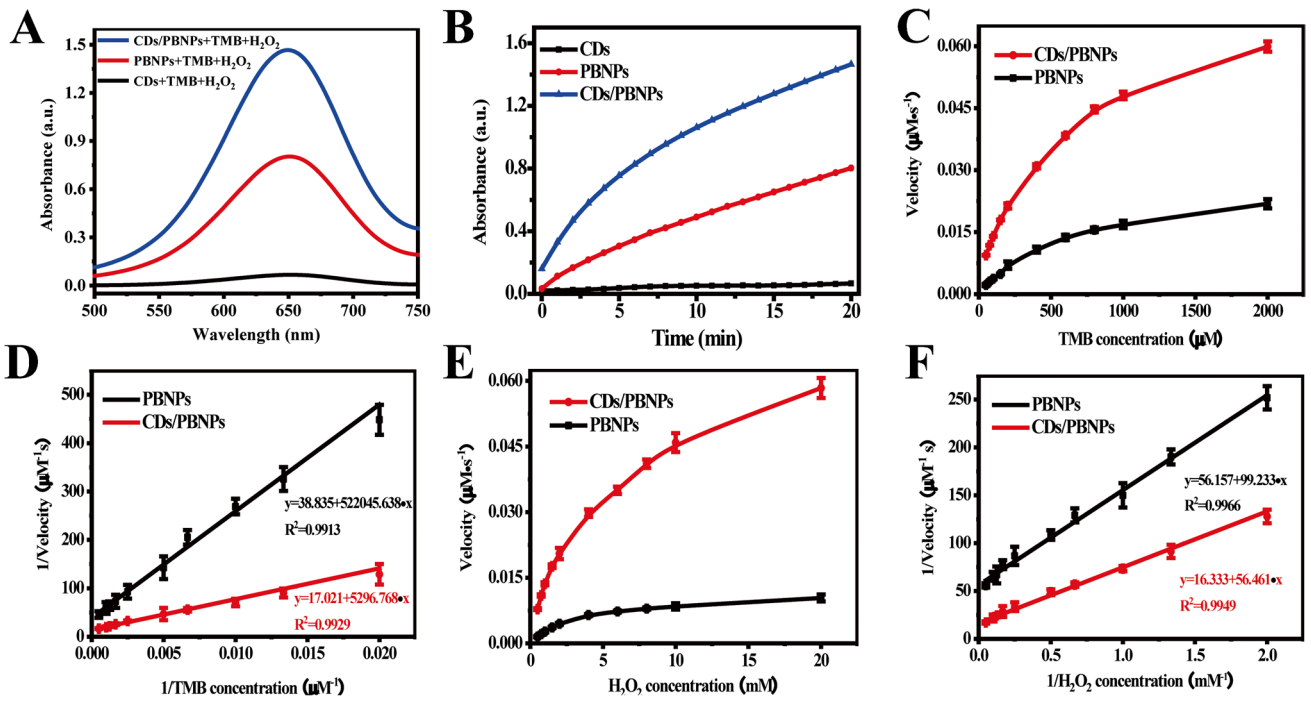

Fig. 3 **A** Absorption spectra of TMBox in different systems: CDs (3 μg/mL) + TMB (1 mM) + H_2O_2 (1 mM); PBNPs (3 μg/mL) + TMB (1 mM) + H_2O_2 (1 mM); CDs/PBNPs (3 μg/mL) + TMB (1 mM) + H_2O_2 (1 mM). **B** Time-dependent absorbance changes of TMBox at 652 nm by the above systems

FL performance in the pH range of 1.0–8.0 (Fig. S10). Additionally, the time-dependent FL intensity of CDs/PBNPs in the presence of Fe^{3+}(1 mM) was showed in Fig. S11. The FL intensity gradually decreased and was stable after 12 min.

The specific quenching effect may be due to the strong interactions between the surface groups of CDs/PBNPs and Fe^{3+}, which destroy the process of radiative transition and lead to the fluorescence quenching [2]. To confirm the quenching mechanism, the UV–vis absorption spectrum and the FL lifetime of CDs/PBNPs in the presence and absence of Fe^{3+} were carefully examined [40]. As shown in Figure S12, the absorption spectrum of CDs/PBNPs-Fe^{3+} (CDs/PBNPs 10 μg/mL, Fe^{3+} 100 μM) system was not overlapped with the sum absorption spectrum of CDs/PBNPs (10 μg/mL) and Fe^{3+} (100 μM), indicating that CDs/PBNPs and Fe^{3+} form ground state complex. This result heralded the quenching mechanism of CDs/PBNPs-Fe^{3+} system was the static quenching. As displayed in Figure S13, the FL decay curves of CDs/PBNPs and CDs/PBNPs + Fe^{3+} systems were almost superposed. And the average FL lifetime calculated by the sum of the $\sum b_i\tau_i$ from the biexponential equation of the two systems (Figure S13 inset). The two FL decay components of CDs/PBNPs (10 μg/mL) were τ_1 4.42 ns (50.45%) and τ_2 8.77 ns (49.55%), and the average FL lifetime was about 6.58 ns. After the addition of Fe^{3+} (100 μM), the two FL decay components changed slightly, τ_1 4.29 ns (45.49%) and τ_2 8.56 ns (54.51%), and the average FL lifetime was about 6.62 ns. The average FL lifetime of CDs/PBNPs and CDs/PBNPs-Fe^{3+} systems were almost constant, indicating that the quenching mechanism between CDs/PBNPs and Fe^{3+} was the static quenching.

Due to the important role of Fe^{3+} ions in various living systems, the detection of Fe^{3+} via a visible fluorescent probe would be of great benefit. As shown in Fig. 4C, with increasing concentration of Fe^{3+}, the FL intensity of CDs/PBNPs gradually decreased, revealing that the FL intensity of CDs/PBNPs is sensitive to the concentration of Fe^{3+}. The Stern–Volmer plot of F_0/F with the corresponding concentration of Fe^{3+} was displayed in Fig. 4D, where F_0 is the FL intensity of CDs/PBNPs without Fe^{3+} and F is the FL intensity of CDs/PBNPs with Fe^{3+} (λ_{ex} = 420 nm and λ_{em} = 510 nm). Over the concentration range of 4–128 μM, the quenching efficiency was commendably consistent with the Stern–Volmer equation:

$$\frac{F_0}{F} = 1 + K_{sv}[Q] \quad (4)$$

where K_{sv} is the Stern–Volmer quenching constant and [Q] is the concentration of Fe^{3+} (Fig. 4D inset). The correlation coefficient (R^2) was as high as 0.9996, and K_{sv} was calculated to be 0.00293. However, the F_0/F curve did not conform to a linear equation in the range of 2 μM–1 mM, indicating that the dynamic quenching process also exists in CDs/PBNPs system [38]. The limit of detection (LOD) was estimated to be 2.0 μM based on a 3/S (is the standard deviation of the blank and S is the slope of the linear regression). Compared with different fluorescent probes for Fe^{3+} detection (Table S1), CDs/PBNPs exhibit high sensitivity.

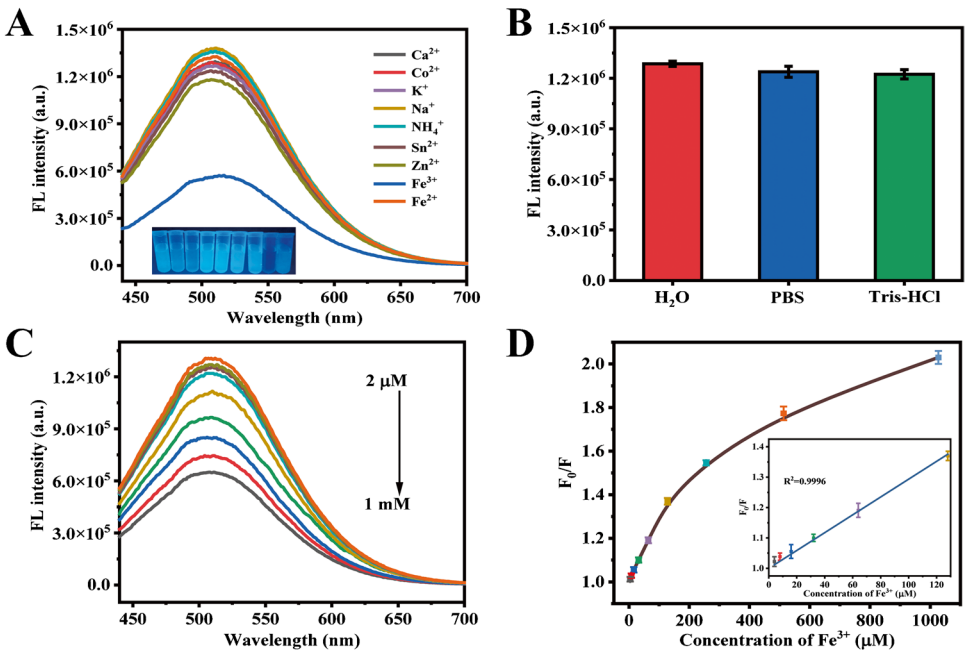

Fig. 4 **A** FL spectra of CDs/PBNPs (10 μg/mL) with different metal ions (1 mM). **B** FL spectra of CDs/PBNPs (10 μg/mL) with different buffer solutions: phosphate buffer saline (PBS), Tris–HCl buffer (Tris–HCl). **C** FL spectra of CDs/PBNPs (10 μg/mL) with different Fe^{3+} concentration (2 μM–1 mM). **D** Stern–Volmer plot of the quenching of the FL of CDs/PBNPs (10 μg/mL) by Fe^{3+}. The inset in (**D**) shows the kinetic plot of the quenching of the FL of CDs/PBNPs (10 μg/mL) by the addition of Fe^{3+} (2 μM–128 μM). Error bar represents the standard deviation for three determinations. All FL spectrums were acquired at the excitation wavelength of 420 nm

Table 2 Results for the determination of Fe^{3+} and free cholesterol in serum samples. Conditions: PBNPs and CDs/PBNPs, 3 μg/mL. $n = 3$

Systems	No	Clinical result (mM)	Found (mM)	Added (mM)	Found (mM)	Recovery (%)	RSD (%)
Fe^{3+}	1	0.0194	0.0188 ± 0.0005	0.01	0.0284 ± 0.0003	96.60	3.21
	2	0.0223	0.0217 ± 0.0003	0.01	0.0325 ± 0.0003	100.61	1.13
	3	0.0237	0.0233 ± 0.0003	0.01	0.0324 ± 0.0004	96.14	3.68
Cholesterol	1	3.87	3.94 ± 0.12	5	8.66 ± 0.21	97.63	2.73
	2	4.15	4.27 ± 0.15	5	8.97 ± 0.18	98.03	3.18
	3	4.38	4.25 ± 0.15	5	9.03 ± 0.14	96.27	2.98

Cooperation interaction of CDs/PBNPs and Fe^{3+}

Various nanomaterials with mimic enzyme activity contain metal ions, such as CuO, V_2O_5, MnO_2, and Co_3O_4 [42–45]. The mimic enzyme activities of these nanomaterials are mainly attributed to metal ions. So, it could be speculated that the addition of Fe^{3+} would also affect the peroxidase-like activity of CDs/PBNPs. To verify this idea, the peroxidase-like activity of CDs/PBNPs in the presence and absence of Fe^{3+} was investigated (Fig. 5A). The UV–vis spectra showed that the system of CDs/PBNPs, Fe^{3+}, TMB, and H_2O_2 exhibited higher peroxidase-like activity than CDs/PBNPs and Fe^{3+}, which was due to the cooperation between CDs/PBNPs and Fe^{3+}. The effects of other ions on the peroxidase-like activity of CDs/PBNPs were also investigated. Nine metal ions including Na^+, K^+, Ca^{2+}, Co^{2+}, Mn^{2+}, Zn^{2+}, Cu^{2+}, Fe^{2+}, and Fe^{3+} were selected in the system of CDs/PBNPs, TMB, and H_2O_2 under the same condition (Fig. 5B). Among these metal ions, Fe^{3+} significantly accelerates the peroxidase-like

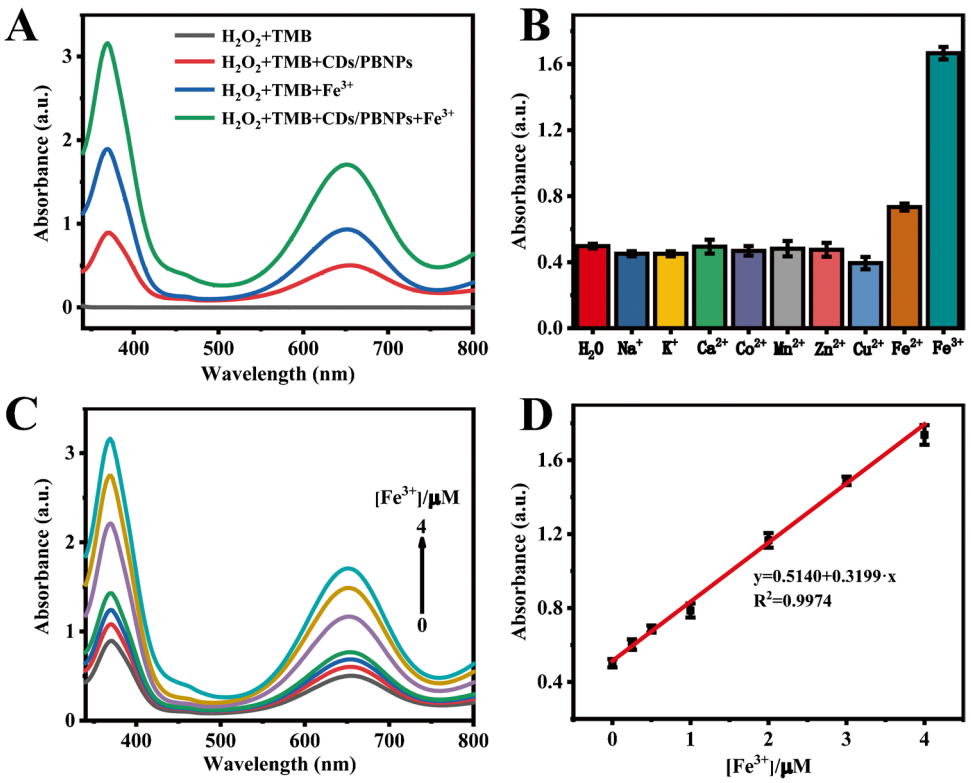

Fig. 5 **A** UV–vis spectra of TMBox in different systems: H_2O_2 + TMB; H_2O_2 + TMB + CDs/PBNPs; H_2O_2 + TMB + Fe^{3+}; H_2O_2 + TMB + CDs/PBNPs + Fe^{3+}. **B** UV–vis spectra of TMBox with different metal ions (4 μM) in the presence of CDs/PBNPs, H_2O_2 and TMB. **C** UV–vis spectra of TMBox with different concentration of Fe^{3+} (0.25–4 μM) in the presence of CDs/PBNPs, H_2O_2, and TMB. **D** The relationship of peroxidase-like activity of CDs/PBNPs and different concentration of Fe^{3+} (0.25–4 μM) by recording UV–vis spectra of TMBox at 652 nm. The concentration of CDs/PBNPs, Fe^{3+}, H_2O_2, and TMB are 10 μg/mL, 10 μg/mL, 2 mM, and 2 mM, respectively. All reaction systems are in 3 mL of HAc-NaAc buffer (0.1 M, pH 7.4). Error bar represents the standard deviation for three determinations. Error bar represents the standard deviation for three determinations

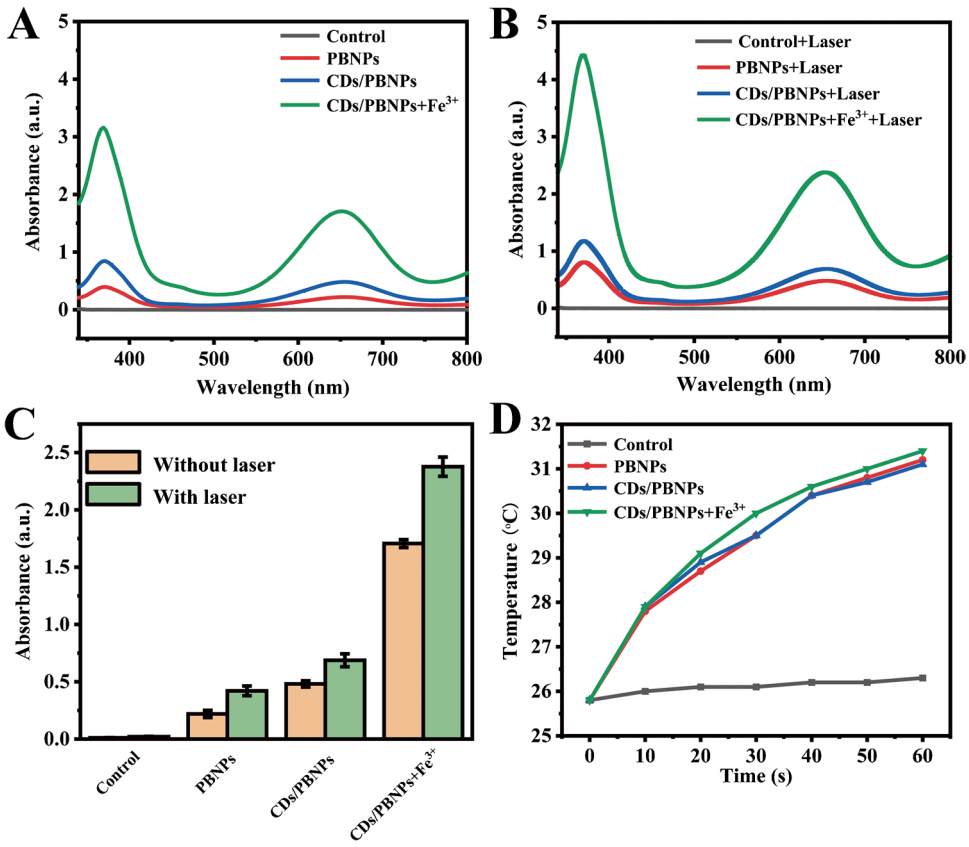

Fig. 6 UV–vis absorption spectra of TMBox without (**A**) and with (**B**) laser in different systems: H_2O_2 + TMB; H_2O_2 + TMB + CDs/PBNPs; H_2O_2 + TMB + Fe^{3+}; H_2O_2 + TMB + CDs/PBNPs + Fe^{3+}. Comparison of the influence of photothermal effect on peroxidase-like activity of PBNPs, CDs/PBNPs, and CDs/PBNPs + Fe^{3+} in H_2O_2-TMB systems by recording the UV–vis absorption spectra of TMBox at 652 nm (**C**). Temperature changes of PBNPs, CDs/PBNPs, and CDs/PBNPs + Fe^{3+} in H_2O_2-TMB systems under laser irradiation (**D**). All experimental data were conducted under the following conditions: the concentrations of Fe^{3+}, PBNPs, CDs/PBNPs, TMB, and H_2O_2 are 4 μg/mL, 10 μg/mL, 10 μg/mL, 2 mM, and 2 mM; all systems are in 3 mL of HAc-NaAc buffer (0.1 M pH 7.4); 808 nm laser (0.75 W/cm^2) was used for the reaction; reaction time is 1 min. Error bar represents the standard deviation for three determinations

activity. Moreover, the higher concentration of Fe^{3+} causes the higher peroxidase-like activity (Fig. 5C and D).

Photothermal-enhanced peroxidase-like activity of PBNPs, CDs/PBNPs, and CDs/PBNPs + Fe^{3+}

According to the Arrhenius formula, nanozymes with near infrared absorption could efficiently convert light energy into heat energy to promote the temperature, which could accelerate the catalytic reaction [25, 26]. CDs/PBNPs have broad absorbance in the near infrared region due to the charge transfer between Fe^{2+} and Fe^{3+} (Fig. 2E). Therefore, the introduction of laser could promote the peroxidase-like activity of CDs/PBNPs. Based on this, the peroxidase-like (Fig. 6A) and photothermal-enhanced peroxidase-like (Fig. 6B) activities of PBNPs, CDs/PBNPs, and CDs/PBNPs + Fe^{3+} were measured by the oxidation of TMB in the presence of H_2O_2. Under 808 nm laser irradiation (0.75 W/cm^2), PBNPs, CDs/PBNPs, and CDs/PBNPs + Fe^{3+} showed enhanced peroxidase-like activities, and CDs/PBNPs + Fe^{3+} exhibited the highest peroxidase-like activity (Fig. 6C). To confirm that the accelerated peroxidase-like activity was due to the photothermal effect, the temperature changes of PBNPs, CDs/PBNPs, and CDs/PBNPs + Fe^{3+} systems were investigated under laser irradiation (Fig. 6D). The temperature of these systems increased about 5 ℃ under laser irradiation, while on temperature change was found in the control group (H_2O_2-TMB system). Moreover, the effect of photothermal and thermal energy on the catalytic reaction was compared (Fig. S14). The result indicated that both the photothermal and thermal effect could enhance the catalytic process, while the effect of temperature change caused by thermal energy on the catalytic reaction was much higher. The reason for this result may be that the temperature of the catalytic system quickly reaches the equilibrium temperature due to the thermal effect. The effect of laser power on

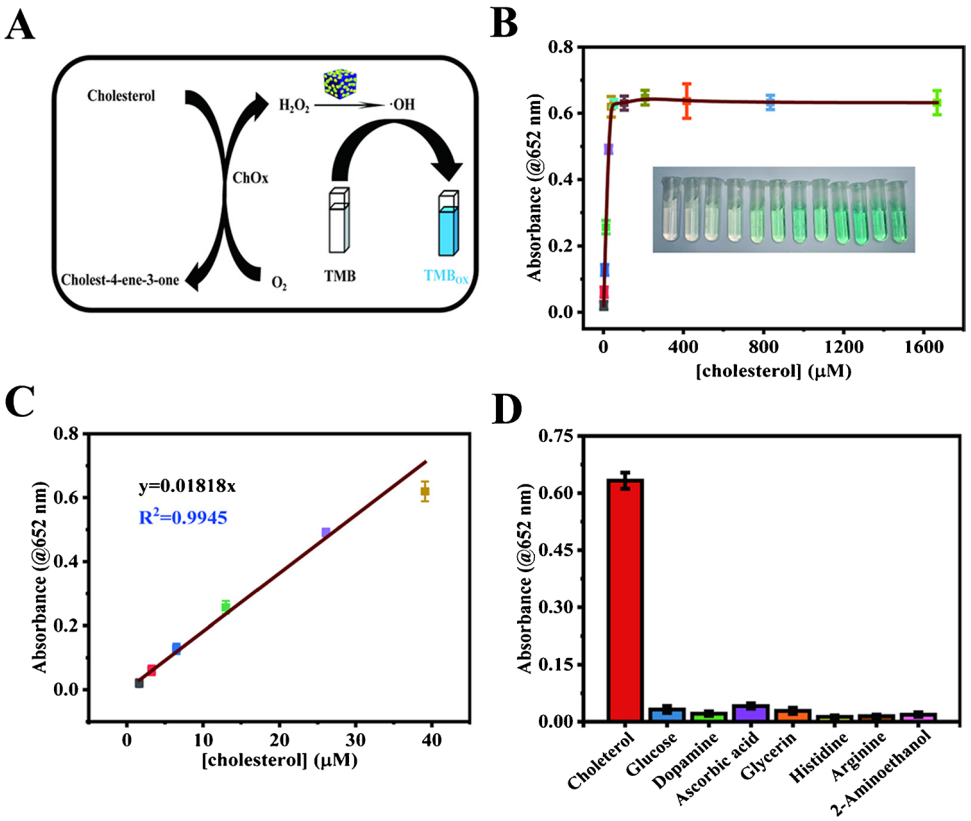

Fig. 7 **A** Schematic illustration of the detection of free cholesterol. **B** Relationship between the concentration of free cholesterol and the absorbance at λ = 652 nm. The inset in (**B**) exhibits the color changes of the cholesterol systems with different concentration (cholesterol concentration increase from left to right). **C** Linear relationship between the concentration of free cholesterol and the absorbance at λ = 652 nm. **D** Changes in absorbance of different species at λ = 652 nm (cholesterol, glucose, dopamine, ascorbic acid, glycerin, histidine, arginine and 2-aminoethanol, 39 μM). Error bar represents the standard deviation for three determinations. All experimental data were conducted under the following conditions: the concentrations of CDs/PBNPs and TMB are 10 μg/mL and 1 mM. All reaction systems are in 3 mL of HAc-NaAc buffer (0.1 M, pH 7.4). Error bar represents the standard deviation for three determinations

the peroxidase-like activity of CDs/PBNPs was also studied (Fig. S15). Under different laser powers (0.5, 0.75, and 1.25 W/cm^2), the peroxidase-like activity of CDs/PBNPs increased with the increase of laser powers. This result was consistent with the changes of temperature (Fig. S16), which further indicated that the photothermal-enhanced peroxidase-like activity was due to the increase of the temperature. Additionally, CDs/PBNPs exhibited excellent photothermal performance under laser irradiation (808 nm, 0.75 W/cm^2) and showed good photothermal stability after 5 irradiation cycles (Fig. S17 and S18), indicating that CDs/PBNPs could be used as a stable photothermal reagent for catalytic reaction.

Detection of free cholesterol

Cholesterol is an important indicator of people's health, and its concentration in blood is of great important for the prevention of many diseases. Note that H_2O_2 is the major product in the reaction between cholesterol oxidase and cholesterol. Therefore, the concentration of cholesterol can be measured using CDs/PBNPs. Cholesterol first reacts with cholesterol oxidase in the presence of O_2. The generated H_2O_2 is catalyzed to produce ·OH under the peroxidase-like of CDs/PBNPs. The ·OH can future oxidize colorless TMB to colored TMBox (Fig. 7A). The level of cholesterol is determined by recording the absorbance of TMBox at 652 nm (Fig. 7B and inset). With increase of cholesterol concentration, the absorption value increases gradually. Note that a linear regression equation ($R^2 = 0.99484$) is fitted in the cholesterol concentration of 2–39 μM (Fig. 7C) and the LOD was measured to be 1.6 μM. Moreover, the selectivity of CDs/PBNPs for the detection of cholesterol was also evaluated (Fig. 7D). The possible interfering species (such as glucose, dopamine, ascorbic acid, glycerin, histidine, arginine and 2-aminoethanol) show no significant effect on the detection of free cholesterol. Compared with other reported assays based on nanomaterials, CDs/PBNPs exhibit the improvement

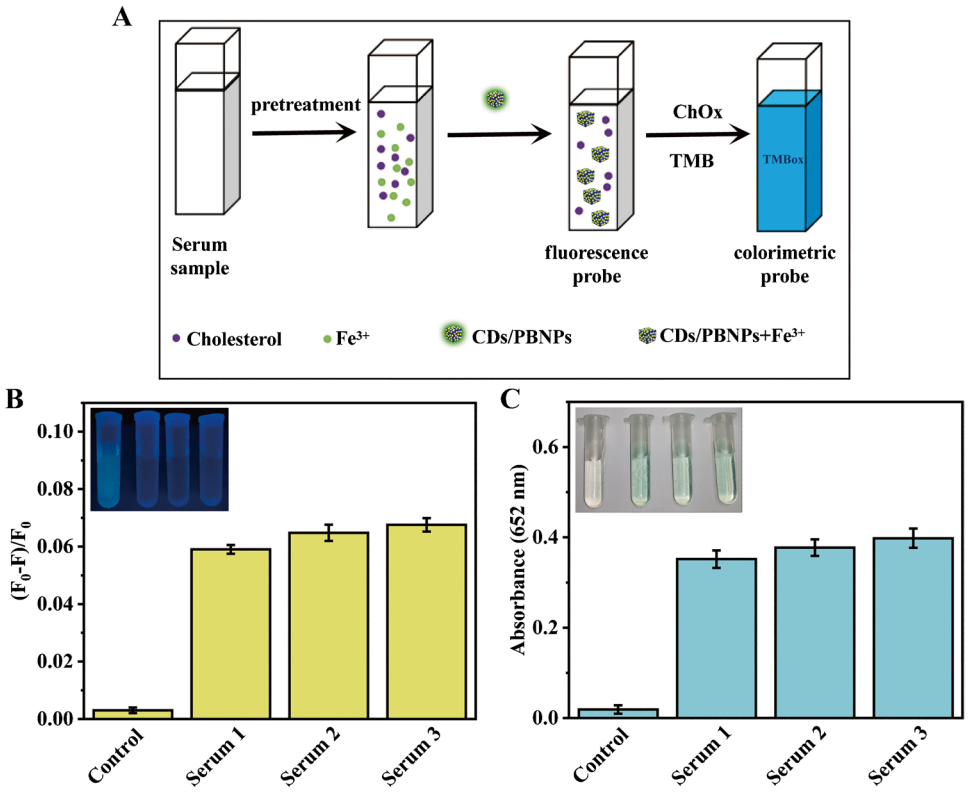

Fig. 8 **A** Schematic illustration of the detection of Fe^{3+} and free cholesterol. **B** Determination of Fe^{3+} (**B**) and cholesterol (**C**) in serum samples. Inset: the corresponding digital images. All experimental data were conducted under the following conditions: the concentration of CDs/PBNPs and TMB are 10 μg/mL and 1 mM. All reaction systems are in 3 mL of HAc-NaAc buffer (0.1 M, pH 7.4). Error bar represents the standard deviation for three determinations

on LOD and the linear range (Table S2). This reveals that CDs/PBNPs have good performance among other nanomaterials.

Application in human serum samples

Based on the above results, a cascade strategy was proposed for detection of Fe^{3+} and cholesterol (Fig. 8A). Serum sample was first nitrated to release the Fe^{3+} from the protein. After adjusting serum sample to neutral, CDs/PBNPs were added as FL probe for detecting Fe^{3+}. Due to the introduction of Fe^{3+}, the peroxidase-like activity of CDs/PBNPs was enhanced. CDs/PBNPs + Fe^{3+} could also serve as colorimetric probe for detection of cholesterol in the present of TMB. As shown in Fig. 8B and 8C, CDs/PBNPs exhibited sensitive detection for Fe^{3+} and cholesterol, which was also proved in the. photographic images (Fig. 8B and 8C inset). Moreover, the obtained results were consistent with the results from Northeast Normal University Hospital (Table 2), suggesting high accuracy and credibility for this method of monitoring Fe^{3+} and cholesterol.

Conclusion

CDs/PBNPs synthesized by a simple and environmentally friendly two-step method exhibit enhanced peroxidase-like activity and FL property. The introduction of Fe^{3+} can not only quench the FL of CDs/PBNPs though the static quenching, but also enhance the peroxidase-like activity of CDs/PBNPs due to the cooperation between CDs/PBNPs and Fe^{3+}. Moreover, under laser irradiation, the peroxidase-like activity of CDs/PBNPs + Fe^{3+} is further accelerated due to the photothermal effect. CDs/PBNPs has utilized as FL and colorimetric probes proposed for sensitive detection of Fe^{3+} and free cholesterol, respectively. Eventually, this strategy is successfully applied to human serum samples, which had great potential for the prevention of diseases caused by Fe^{3+} and cholesterol.

Supplementary Information The online version contains supplementary material available at https://doi.org/10.1007/s00604-021-05129-w.

Funding This work was supported by the National Natural Science Foundation of China (11774048) and the Project from Key Laboratory for UV-Emitting Materials and Technology of Ministry of Education (No. 130028723). Innovative research group project of the national natural science foundation of china, 11774048,Guiye Shan

Declarations

Conflict of interest The authors declare no competing interests.

References

1. Han C, Wang R, Wang K, Xu H, Sui M et al (2016) Highly fluorescent carbon dots as selective and sensitive "on-off-on" probes for iron(III) ion and apoferritin detection and imaging in living cells. Biosens Bioelectron 83:229–236. https://doi.org/10.1016/j.bios.2016.04.066
2. Atchudan R, Edison T, Aseer KR, Perumal S, Karthik N, Lee YR (2018) Highly fluorescent nitrogen-doped carbon dots derived from Phyllanthus acidus utilized as a fluorescent probe for label-free selective detection of Fe(3+) ions, live cell imaging and fluorescent ink. Biosens Bioelectron 99:303–311. https://doi.org/10.1016/j.bios.2017.07.076
3. Xue J, Tian LM, Yang ZY (2019) A novel rhodamine-chromone Schiff-base as turn-on fluorescent probe for the detection of Zn(II) and Fe(III) in different solutions. J Photochem Photobiol A Chem 369:77–84. https://doi.org/10.1016/j.jphotochem.2018.10.026
4. Wisitsoraat A, Sritongkham P, Karuwan C, Phokharatkul D, Maturos T et al (2010) Fast cholesterol detection using flow injection microfluidic device with functionalized carbon nanotubes based electrochemical sensor. Biosens Bioelectron 26(4):1514–1520. https://doi.org/10.1016/j.bios.2010.07.101
5. Hayat A, Haider W, Raza Y, Marty JL (2015) Colorimetric cholesterol sensor based on peroxidase like activity of zinc oxide nanoparticles incorporated carbon nanotubes. Talanta 143:157–161. https://doi.org/10.1016/j.talanta.2015.05.051
6. Bui TT, Park SY (2016) A carbon dot–hemoglobin complex-based biosensor for cholesterol detection. Green Chem 18(15):4245–4253. https://doi.org/10.1039/c6gc00507a
7. He Y, Niu X, Shi L, Zhao H, Li X et al (2017) Photometric determination of free cholesterol via cholesterol oxidase and carbon nanotube supported Prussian blue as a peroxidase mimic. Microchim Acta 184(7):2181–2189. https://doi.org/10.1007/s00604-017-2235-y
8. Kivipelto M, Helkala EL, Laakso MP, Hanninen T, Hallikainen M et al (2002) Apolipoprotein E epsilon 4 allele, elevated midlife total cholesterol level, and high midlife systolic blood pressure are independent risk factors for late-life Alzheimer disease. Ann Intern Med 137(3):149–155. https://doi.org/10.7326/0003-4819-137-3-200208060-00006
9. Li ZX, Li HX, Shi CX, Yu MM, Wei LH et al (2016) Nanomolar colorimetric quantitative detection of Fe^{3+} and PPi with high selectivity. Spectrochim Acta A Mol Biomol Spectrosc 159:249–253. https://doi.org/10.1016/j.saa.2016.02.001
10. Nirala NR, Abraham S, Kumar V, Bansal A, Srivastava A et al (2015) Colorimetric detection of cholesterol based on highly efficient peroxidase mimetic activity of graphene quantum dots. Sens Actuators B 218:42–50. https://doi.org/10.1016/j.snb.2015.04.091
11. Jiang YL, Han QR, Jin C, Zhang J, Wang BX (2015) A fluorescence turn-off chemosensor based on N-doped carbon quantum dots for detection of Fe^{3+} in aqueous solution. Mater Lett 141:366–368. https://doi.org/10.1016/j.matlet.2014.10.168
12. Bui TT, Park SY (2016) A carbon dot-hemoglobin complex-based biosensor for cholesterol detection. Green Chem 18(15):4245–4253. https://doi.org/10.1039/c6gc00507a
13. Lee YJ, Park JY (2010) Nonenzymatic free-cholesterol detection via a modified highly sensitive macroporous gold electrode with platinum nanoparticles. Biosens Bioelectron 26(4):1353–1358. https://doi.org/10.1016/j.bios.2010.07.048
14. Nguyen LD, Doan TCD, Huynh TM, Dang DMT, Dang CM (2021) Thermally reduced graphene/nafion modified platinum disk electrode for trace level electrochemical detection of iron. Microchem 169:106627. https://doi.org/10.1016/j.microc.2021.106627
15. Andersen JET (2005) A novel method for the filterless preconcentration of iron. Analyst 130(3):385–390. https://doi.org/10.1016/j.microc.2021.106627
16. Peng X, Wang R, Wang T, Yang W, Wang H, Gu W et al (2018) Carbon dots/Prussian blue satellite/core nanocomposites for optical imaging and photothermal therapy. ACS Appl Mater Interfaces 10(1):1084–1092. https://doi.org/10.1021/acsami.7b14972
17. Zhou J, Li M, Hou Y, Luo Z, Chen Q et al (2018) Engineering of a nanosized biocatalyst for combined tumor starvation and low-temperature photothermal therapy. ACS Nano 12(3):2858–2872. https://doi.org/10.1021/acsnano.8b00309
18. Fu GL, Liu W, Li YY, Jiang LG, Liang XL et al (2014) Magnetic Prussian blue nanoparticles for targeted photothermal therapy under magnetic resonance imaging guidance. Bioconjug Chem 25(9):1655–1663. https://doi.org/10.1021/bc500279w
19. Li WP, Su CH, Tsao LC, Chang CT, Hsu YP et al (2016) Controllable CO-release following near-infrared light-induced cleavage of iron carbonyl derivatized Prussian blue nanoparticles for CO-assisted synergistic treatment. ACS Nano 10(12):11027–11036. https://doi.org/10.1021/acsnano.6b05858
20. Kim T, Lemaster JE, Chen F, Li J, Jokerst JV (2017) Photoacoustic imaging of human mesenchymal stem cells labeled with Prussian blue-poly(l-lysine) na-nocomplexes. ACS Nano 11(9):9022–9032. https://doi.org/10.1021/acsnano.7b03519
21. Zhou D, Zeng K, Yang M (2019) Gold nanoparticle-loaded hollow Prussian blue nanoparticles with peroxidase-like activity for colorimetric determination of L-lactic acid. Microchim Acta 186(2):121. https://doi.org/10.1007/s00604-018-3214-7
22. Chen J, Wang Q, Huang L, Zhang H, Rong K, Zhang H et al (2018) Prussian blue with intrinsic heme-like structure as peroxidase mimic. Nano Res 11(9):4905–4913. https://doi.org/10.1007/s12274-018-2079-8
23. Komkova MA, Karyakina EE, Karyakin AA (2018) Catalytically synthesized Prussian blue nanoparticles defeating natural enzyme peroxidase. J Am Chem Soc 140(36):11302–11307. https://doi.org/10.1021/jacs.8b05223
24. Zhang W, Hu S, Yin JJ, He W, Lu W, Ma M et al (2016) Prussian blue nanoparticles as multienzyme mimetics and reactive oxygen species scavengers. J Am Chem Soc 138(18):5860–5865. https://doi.org/10.1021/jacs.5b12070
25. Li SS, Shang L, Xu BL, Wang SH, Gu K et al (2019) A nanozyme with photo-ehanced dual enzyme-like activities for deep pancreatic cancer therapy. Angew Chem Int Edit 58(36):12631–12624. https://doi.org/10.1002/anie.201904751
26. Zhao YY, Yang J, Shan GY, Liu ZY, Cui AN et al (2020) Photothermal-enhanced tandem enzyme-like activity of $Ag_{2-x}Cu_xS$ nanoparticles for one-step colorimetric glucose detection in unprocessed human urine. Sens Actuators B 305:127420. https://doi.org/10.1016/j.snb.2019.127420
27. Wang C, Ren GY, Yuan BB, Zhang W, Liu MJ et al (2020) Enhancing enzyme-like activities of prussian blue analog nanocages by molybdenum doping: toward cytoprotecting and online optical hydrogen sulfide monitoring. Anal Chem 92(11):7822–7830. https://doi.org/10.1021/acs.analchem.0c01028
28. Lin LP, Luo YX, Tsai P, Wang JJ, Chen X (2018) Metal ions doped carbon quantum dots: synthesis, physicochemical properties, and their applications. Tr-AC Trends Anal Chem 103:87–101. https://doi.org/10.1016/j.trac.2018.03.015
29. Yan FY, Jiang YX, Sun XD, Bai ZJ, Yan Z et al (2018) Surface modification and chemical functionalization of carbon dots: a

review. Microchim Acta 185(9):1–34. https://doi.org/10.1007/s00604-018-2953-9
30. Liu WJ, Li C, Ren YJ, Sun XB, Pan W et al (2016) Carbon dots: surface engineering and applications. J Mater Chem B 4(35):5772–5788. https://doi.org/10.1039/c6tb00976j
31. Shen LM, Liu J (2016) New development in carbon quantum dots technical applications. Talanta 156:245–256. https://doi.org/10.1016/j.talanta.2016.05.028
32. Gul U, Kanwal S, Tabassum S, Gilani MA, Rahim A (2020) Microwave-assisted synthesis of carbon dots as reductant and stabilizer for silver nanoparticles with enhanced-peroxidase like activity for colorimetric determination of hydrogen p-eroxide and glucose. Microchim Acta 187(2):135. https://doi.org/10.1007/s00604-019-4098-x
33. Li YC, Zhong YM, Zhang YY, Wen W, Li SX (2015) Carbon quantum dots/octahedral Cu_2O nanocomposites for non-enzymatic glucose and hydrogen peroxide amperometric. sensor. Sen Actuators B 206:735–743. https://doi.org/10.1016/j.snb.2014.09.016
34. Silva JCGED, Gonçalves HMR (2011) Analytical and bioanalytical applications of carbon dots. TrAC-Trend Anal Chem 30(8):1327–1336. https://doi.org/10.1016/j.trac.2011.04.009
35. Hola K, Zhang Y, Wang Y, Giannelis EP, Zboril R et al (2014) Carbon dots-Emerging light emitters for bioimaging, cancer therapy and optoelectronics. Nano Today 9(5):590–603. https://doi.org/10.1016/j.nantod.2014.09.004
36. De B, Karak N (2017) Recent progress in carbon dot-metal based nanohybrids for photochemical and electrochemical applications. J Mater Chem A 5(5):1826–1859. https://doi.org/10.1039/c6ta10220d
37. Hassan M, Gomes VG, Dehghani A, Ardekani SM (2017) Engineering carbon quantum dots for photomediated theranostics. Nano Res 11(1):1–41. https://doi.org/10.1007/s12274-017-1616-1
38. Liu W, Diao HP, Chang HH, Wang HJ, Li TT et al (2017) Green synthesis of carbon dots from rose-heart radish and application for Fe^{3+} detection and cell imaging. Sen Actuators B 241:190–198. https://doi.org/10.1016/j.snb.2016.10.068
39. Feng H, Qian Z (2018) Functional carbon quantum dots: a versatile platform for chemosensing and biosensing. Chem Rec 18(5):491–505. https://doi.org/10.1002/tcr.201700055
40. Zu FL, Yan FY, Bai ZJ, Xu JX, Wang YY et al (2017) The quenching of the fluorescence of carbon dots: a review on mechanisms and applications. Microchim Acta 184(7):1899–1914. https://doi.org/10.1007/s00604-017-2318-9
41. Koncki R, Wolfbeis OS (1998) Composite films of Prussian Blue and N-substituted polypyrroles: fabrication and application to optical adetermination of pH. Anal Chem 70(13):2533–2550. https://doi.org/10.1021/ac9712714
42. Deng H, Zheng X, Wu Y, Shi X, Lin X et al (2017) Alkaline peroxidase activity of cupric oxide nanoparticles and its modulation by ammonia. Analyst 142(20):3986–3992. https://doi.org/10.1039/c7an01293d
43. Zeb A, Xie X, Yousaf A, Imran M, Wen T et al (2016) Highly efficient Fenton and enzyme-mimetic activities of mixed phase VOx nanoflakes. ACS A-ppl Mater Interfaces 8(44):30126–30132. https://doi.org/10.1021/acsami.6b09557
44. Liu J, Meng LJ, Fei ZF, Dyson PJ, Jing XN et al (2017) MnO_2 nanosheets as an artificial enzyme to mimic oxidase for rapid and sensitive detection of glutathione. Biosens Bioelectron 90:69–74. https://doi.org/10.1016/j.bios.2016.11.046
45. Fan S, Zhao M, Ding L, Li H, Chen S (2017) Preparation of Co_3O_4/crumpled grapheme microsphere as peroxidase mimetic for colorimetric assay of ascorbic acid. Biosens Bioelectron 89:846–852. https://doi.org/10.1016/j.bios.2016.09.108

Publisher's note Springer Nature remains neutral with regard to jurisdictional claims in published maps and institutional affiliations.